

# Comparison of Pauli projection and supersymmetric transformation methods for three-body nuclear structure and reactions

A. Deltuva

*Institute of Theoretical Physics and Astronomy, Vilnius University, Saulėtekio al. 3, LT-10257 Vilnius, Lithuania*  
(Received November 26, 2025)

Three-body Faddeev-type equations for bound, resonant, and scattering states in the systems of nuclear core and two nucleons are solved using the momentum-space framework. Two approaches for eliminating the Pauli-forbidden deeply-bound states are compared, projecting out those states by a nonlocal term in the potential, and by a supersymmetric transformation of the potential. While the former method is preferred by the experimental data for the deuteron- ${}^4\text{He}$  scattering, the results for bound and resonant states do not indicate a clear superiority of a single method. Instead, systematic differences between them are found.

## I. INTRODUCTION

Understanding the nuclear structure and reactions in terms of simplified few-body models is among the major goals of nuclear physics. This introduces effective degrees of freedom such as clusters of  $\alpha$  particles or nuclear core plus external nucleons, whose interactions are described by effective two-body (and possibly three-body) potentials, with parameters fitted to binding or low-energy scattering data. The fermionic character of a many-body nuclear system plays a crucial role, demanding to impose the constraints of the antisymmetry for the nuclear wave functions. The deepest bound states supported by those effective potentials correspond to the states implicitly occupied by the internal core nucleons, and thus are Pauli forbidden for external nucleons. In simple approaches to nuclear reactions such as the distorted-wave Born approximation (DWBA) and adiabatic distorted-wave approximation (ADWA) [1] only the core plus nucleon bound-state wave functions are needed that are simply taken for the desired energy level. The problem of Pauli-forbidden states becomes more serious in full three-body calculations, where the external nucleons cannot occupy those deep states embedded into three-body space. Without affecting higher-lying (Pauli allowed) and continuum states, this restriction can be implemented in several ways: (i) the Pauli-forbidden states are projected out from the considered model space; this can be achieved by adding a strong repulsive nonlocal projection term to the two-body potential [2–4] or, in the adiabatic expansion method [5, 6], omitting the subset of states corresponding to Pauli-forbidden states; (ii) the supersymmetric (SS) transformation is applied to the potential [7] creating a repulsive  $r^{-2}$  term, that eliminates the deepest states but keeps all the higher states unchanged. A less sophisticated variation of (ii) is a potential with repulsive core (RC) [4], that however does not preserve exact phase equivalence to the original potential.

The Pauli projection (PP) and SS transformation methods have been compared in several works. Hesse et al. [8] calculated weakly bound two-neutron halo nuclei  ${}^6\text{He}$ ,  ${}^{11}\text{Li}$ , and  ${}^{14}\text{Be}$ . They found that SS type potentials yield more binding, but after the potential rescaling to

fit the same binding energy the radii obtained with PP and SS methods turn out to be very close. Garrido et al. [6] studied  ${}^6\text{He}$  and  ${}^{11}\text{Li}$  and arrived to similar conclusions. Thompson et al. [4] considered  ${}^6\text{He}$  and  ${}^6\text{Be}$  systems, revealing no significant differences between several treatments of Pauli forbidden states in bound and resonant states, but visible effects for nonresonant continuum. For example, the dipole distribution for  ${}^6\text{He}$  calculated in the SS method was systematically higher than in the PP method, though the shape was similar.

The most detailed study of the continuum is offered by exclusive scattering processes. The continuum of the  ${}^4\text{He}$  core and two nucleons was considered in Ref. [9] on the examples of the deuteron- ${}^4\text{He}$  elastic scattering and breakup, revealing very large differences between the PP and RC models for the nucleon- ${}^4\text{He}$  potential, not only in magnitude but also in shape, with the experimental data clearly preferring the PP model. As the SS method was not implemented, it remained unclear whether the findings were not due to the violation of the phase equivalence. This question will be sorted out in the present work using rigorous Faddeev-type scattering equations for transition operators [9, 10], solved in the momentum space. Note that due to high excitation energy of  ${}^4\text{He}$  this is one of few systems involving composite nuclei that is described not by optical but real potentials in the continuum. The complex potentials do not support real bound states, and therefore are excluded from the discussion.

Regarding the bound states, the comparison of the PP and SS models will be performed not only for weakly bound two-neutron halo nuclei such as  ${}^{11}\text{Li}$  and  ${}^{19}\text{B}$  but also for more tightly bound systems accommodating bound excited states such as  ${}^{16}\text{C}$  and  ${}^{18}\text{O}$ . The aim is not to fit their binding energies but to study the emergence of differences between the PP and SS and possibly find a systematic pattern.

Finally, the unbound  ${}^{16}\text{Be}$  nucleus will be studied. This will demonstrate the ability of the momentum-space transition operator method to determine the resonance properties for core plus two-neutron systems. Furthermore, it appears that existing  ${}^{16}\text{Be}$  calculations [11, 12] performed in the coordinate space rely on the SS model, presumably taking advantage of its local form, in contrast to the nonlocal PP potentials. In the momentum-space

integral equation framework both local and nonlocal potentials are treated on the same footing.

Section II shortly recalls the description of three-body bound and scattering states using transition operators together with the essential aspects of calculations. Section III presents results scattering observables, bound state properties and resonances. Discussion and conclusions are collected in Sec. VI.

## II. THREE-BODY BOUND-STATE AND CONTINUUM EQUATIONS

Faddeev equations [13] employ the decomposition of the three-body wave function  $|\Psi\rangle = \sum_{\alpha=1}^3 |\psi_{\alpha}\rangle$  into the amplitudes  $|\psi_{\alpha}\rangle$ . For the three-body bound state with energy  $E_B < 0$  (measured from the threshold of three free particles) the Faddeev amplitudes obey the system of coupled equations

$$|\psi_{\alpha}\rangle = G_0(E_B) \sum_{\beta=1}^3 \bar{\delta}_{\alpha\beta} T_{\beta}(E_B) |\psi_{\beta}\rangle. \quad (1)$$

The Greek subscripts label the spectator particle in the odd-man-out notation,  $\bar{\delta}_{\alpha\beta} = 1 - \delta_{\alpha\beta}$ ,

$$G_0(Z) = (Z - H_0)^{-1} \quad (2)$$

is the free resolvent with the kinetic energy operator  $H_0$ , and

$$T_{\alpha}(Z) = v_{\alpha} + v_{\alpha} G_0(Z) T_{\alpha}(Z) \quad (3)$$

is the two-particle transition operator acting in the three-body space, with  $v_{\alpha}$  being the corresponding two-particle potential.

The transition operators  $U_{\beta\alpha}(Z)$  in the Alt-Grassberger-Sandhas version [10] obey the system

$$U_{\beta\alpha}(Z) = \bar{\delta}_{\beta\alpha} [G_0(Z)]^{-1} + \sum_{\eta=1}^3 \bar{\delta}_{\beta\eta} T_{\eta}(Z) G_0(Z) U_{\eta\alpha}(Z). \quad (4)$$

The physical amplitudes for reactions at energy  $E$  are obtained as on-shell matrix elements of the transition operators  $U_{\beta\alpha}(E + i0)$ , see Ref. [9] for the definitions of deuteron- ${}^4\text{He}$  elastic and breakup amplitudes. At  $Z = E_B$  the transition operators  $U_{\beta\alpha}(E_B)$  have the bound-state pole, while three-body resonances, if existing, correspond to poles of  $U_{\beta\alpha}(Z_R)$  at  $Z_R = E_R - i\Gamma/2$  in the second Riemann sheet of the complex energy plane, with the resonance position  $E_R$  and width  $\Gamma$ . If the resonance is not very broad, those parameters can be determined from the energy dependence of matrix elements obtained at real physical energies as done in the fictitious three-neutron system with enhanced interactions [14], i.e.,

$$U_{\beta\alpha}(E + i0) \approx \frac{\tilde{U}_{\beta\alpha}^{(-1)}}{E - E_R + i\Gamma/2} + \tilde{U}_{\beta\alpha}^{(0)} + \dots \quad (5)$$

The equations (1) and (4) are solved in the momentum-space partial-wave representation. Three sets of basis functions  $|p_{\alpha} q_{\alpha}(l_{\alpha}\{[L_{\alpha}(s_{\beta} s_{\gamma}) S_{\alpha}] j_{\alpha} s_{\alpha}\} \mathcal{S}_{\alpha}) JM\rangle$  are used with  $(\alpha, \beta, \gamma)$  being cyclic permutations of (1, 2, 3). The Jacobi momenta  $p_{\alpha}$  and  $q_{\alpha}$  refer to the pair  $(\beta, \gamma)$  and spectator  $\alpha$ , their associated orbital angular momenta are  $L_{\alpha}$  and  $l_{\alpha}$ . Together with the particle spins  $s_{\alpha}, s_{\beta}, s_{\gamma}$  they are coupled to the total angular momentum  $J$ ,  $M$  being its projection.  $S_{\alpha}$  and  $j_{\alpha}$  are the spin and total angular momentum of the pair  $\alpha$ , and  $\mathcal{S}_{\alpha}$  is the three-body channel spin. In the core plus two-neutron systems including partial waves with  $L_{\alpha} \leq 3$  leads to well converged results. However, if a proton is involved such as in the deuteron- ${}^4\text{He}$  scattering, the screening and renormalization method [15–17] for the inclusion of the Coulomb force requires screening radii up to 20 fm and, consequently,  $L_{\alpha}$  up to 15 for the proton- ${}^4\text{He}$  pair.

## III. RESULTS

The two-nucleon interaction is taken to be the high-precision charge-dependent Bonn (CD Bonn) potential [18], though any realistic two-nucleon potential leads to a very similar results as proven in a number of previous works, e.g., [9, 19]. The nucleon-nucleus potential is assumed to be of the standard Woods-Saxon form with the spin-orbit term, in the coordinate space given by

$$v(r) = -V_c f(r, R, a) + \mathbf{s}_{\mathbf{N}} \cdot \mathbf{L} V_{so} \frac{1}{r} \frac{d}{dr} f(r, R, a), \quad (6)$$

with  $f(r, R, a) = [1 + \exp((r - R)/a)]^{-1}$ , the diffuseness  $a$  and radius  $R = r_0 A^{1/3}$ . The strengths  $V_c$  and  $V_{so}$  are adjusted case by case and may be partial-wave dependent; for brevity the spectator label  $\alpha$  will be suppressed in the further notation. The interaction is assumed to be independent of the core spin.

If the potential (6) supports a Pauli-forbidden state  $|\phi_P^{Lj}\rangle$ , projecting it out is equivalent to moving to infinitely high energy [3] via modified potential containing a nonlocal projection term,

$$v^P = v + |\phi_P^{Lj}\rangle \Gamma_P \langle \phi_P^{Lj}|. \quad (7)$$

Formally  $\Gamma_P \rightarrow \infty$ , but practically that limit is reached with  $\Gamma_P$  ranging from 1 to 10 GeV, where the predictions to a good accuracy become independent of  $\Gamma_P$ .

In the SS method the potential acquires a local repulsive correction [7] that at short distances behaves like  $r^{-2}$  but, except for the Pauli-forbidden state, has the same spectrum as the original potential. The singular term of the SS potential becomes harmless after transformation to the momentum space.

### A. Deuteron- ${}^4\text{He}$ scattering

The deuteron- ${}^4\text{He}$  elastic scattering and breakup reactions have been studied in Ref. [9]. The comparison of

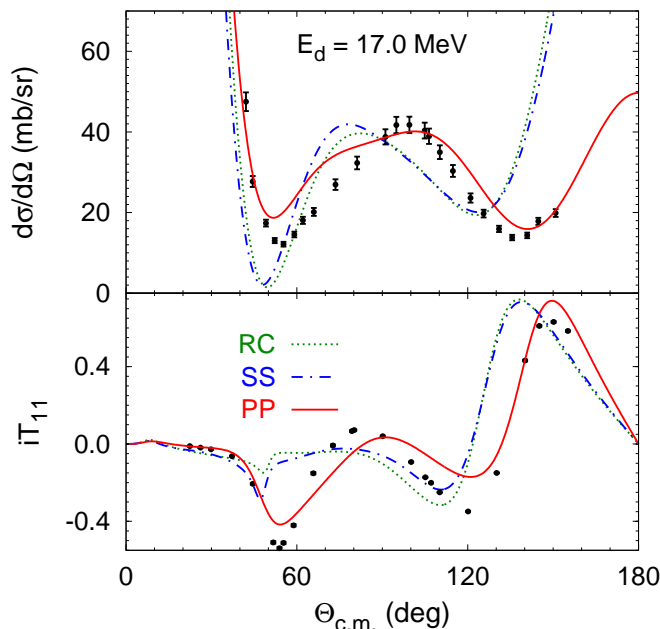


FIG. 1. (Color online) The differential cross section and deuteron vector analyzing power  $iT_{11}$  for the deuteron- $^4\text{He}$  elastic scattering at 17 MeV deuteron beam energy as functions of the c.m. scattering angle. Results of PP (solid curves), SS (dashed-dotted curves), and RC (dotted curves) models are compared. The experimental data are from Ref. [20].

the PP and RC models in Ref. [9] clearly revealed the superiority of the former in reproducing the experimental data. Though both SS and RC potentials are local, the RC potential remains finite at the origin while the SS one has singularity, thus, it is not clear to what extent their predictions will differ, and whether SS will be able to remedy the defects of RC. Figures 1 - 3 present the comparison of predictions using PP, SS, and RC potentials, with their parameters given in Ref. [4], labeled as PP, PS, and PC models there, respectively. They are defined for  $L \leq 2$  partial waves. All the shown examples, i.e., the differential cross section and the deuteron vector analyzing power in the deuteron- $^4\text{He}$  elastic scattering at 17 MeV deuteron beam energy in Fig. 1, the fully exclusive fivefold differential cross section for the deuteron breakup at 15 MeV  $^4\text{He}$  beam energy in Fig. 2, and the differential cross section for the semi-inclusive breakup reaction  $^4\text{He}(d, p)$  in Fig. 3 deliver the same message: the predictions of RC and SS models are quite close to each other and clearly different from the PP ones. The available experimental data [20, 21] favor the PP model, as already found in Ref. [9] where more examples are given. There is no data available for the semi-inclusive reaction  $^4\text{He}(d, p)$ , but it serves as a global characteristic for the breakup in the whole phase space. It has quite a significant contribution from the  $^5\text{He}$  resonant state  $1p_{3/2}$ .

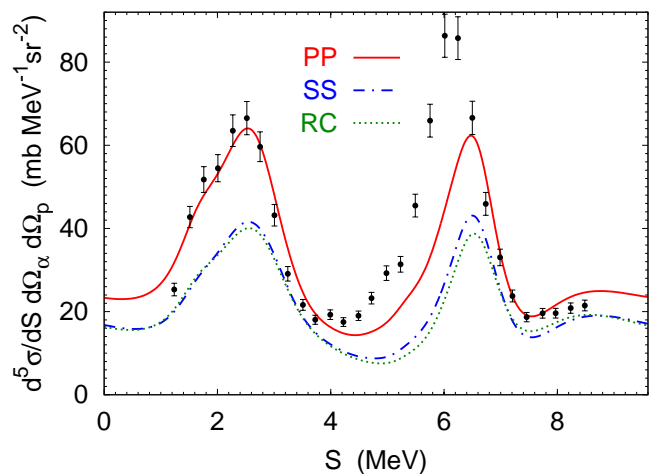


FIG. 2. (Color online) The fully exclusive differential cross section for the deuteron breakup in collision with the 15 MeV  $^4\text{He}$  nucleus. It is shown as a function of the arclength  $S$  along the kinematical curve in a coplanar kinematical configuration with 17.1 and 50.5 deg polar angles of  $^4\text{He}$  and proton, respectively, and with 180 deg difference in their azimuthal angles. Curves are as in Fig. 1, and the experimental data are taken from Ref. [21].

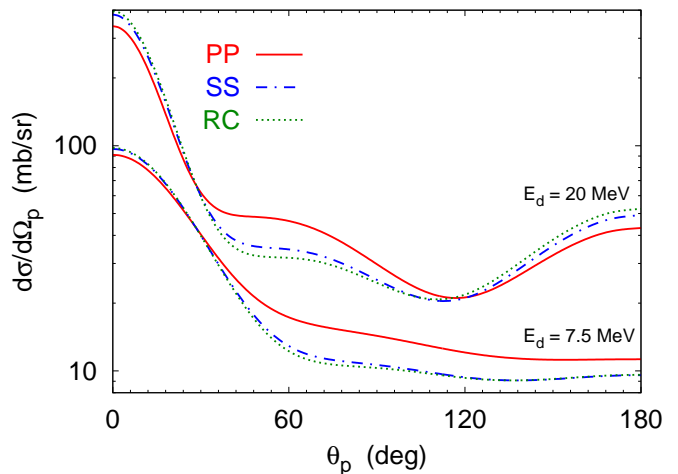


FIG. 3. (Color online) The semi-inclusive differential cross section for the  $^4\text{He}(d, p)$  reaction at 7.5 and 20 MeV deuteron beam energies as a function of the proton scattering angle in the c.m. frame. Curves are as in Fig. 1.

The difference between the PP and SS/RC models to a lesser extent shows up also in the binding energy of  $^6\text{Li}$ , with the predictions (relative to the core plus nucleons threshold) being 3.48, 3.66, and 3.65 MeV, respectively, quite close to the experimental value of 3.69 MeV.

Some potential models project out not the deep state wave function but the ground state of the harmonic oscillator (HO) [22]. As discussed in Ref. [9] this does not lead to a significant difference as compared to the PP

method. Kamada *et al.* [23] calculated the forbidden (called ghost) state microscopically and found that it can be approximated quite well by the HO function with the shell model mode  $\Omega = 0.245 \text{ fm}^{-2}$ . The potential used in this work prefers a smaller value of  $\Omega \approx 0.21 \text{ fm}^{-2}$ , in a good agreement with Ref. [22].

### B. Bound states

Systems consisting of a nuclear core and two neutrons have been extensively studied in the past using three-body models, e.g., in Refs. [4, 8, 24–30]. The used neutron-core interaction models range from PP to SS and RC, though quite often just a single model was chosen. In this section the comparison of PP and SS model will be presented for several nuclei, ranging from weakly to tightly bound. The potential parameters in Eq. (6) are taken from previous works where available. All potentials support Pauli-forbidden  $L = 0$  and 1 states, i.e.,  $1s_{1/2}$  and  $1p_j$ , and no such states for higher  $L$ .

The case of  $n$ - $^9\text{Li}$  is exceptional in the sense that only  $1p_{3/2}$  is Pauli forbidden, while its  $1p_{1/2}$  state is not Pauli-forbidden but resonant. For  $n$ - $^9\text{Li}$  the model P4 of Ref. [24] is taken. It has a virtual  $2s_{1/2}$  state. The parameters were tuned in Ref. [24] to reproduce  $^{11}\text{Li}$  binding energy of 0.3 MeV in the PP treatment.

For  $n$ - $^{17}\text{B}$  the spin-orbit force and  $L$ -dependence is neglected as in Ref. [29], while  $V_c = 42.232 \text{ MeV}$ ,  $R = 3 \text{ fm}$ ,  $a = 0.6 \text{ fm}$ , reproducing a virtual  $2s_{1/2}$  state with large negative two-body scattering length of  $-100 \text{ fm}$  [29].

For  $n$ - $^{18}\text{C}$  the parameters are taken from DPp model Ref. [28], supporting a bound  $2s_{1/2}$  state with  $E_B = -0.58 \text{ MeV}$ . The potential has no spin-orbit force and uses the same parameters in all waves.

For  $n$ - $^{14}\text{C}$  the parameters are taken from Ref. [19], adjusted to the low-energy spectrum of  $^{15}\text{C}$  and neutron separation energy of  $^{14}\text{C}$ .

For  $n$ - $^{16}\text{O}$  the parameters are taken from Ref. [30], again adjusted to the low-energy spectrum of  $^{17}\text{O}$ . Since they are defined for  $L \leq 2$  partial waves, the results presented in Tables will use  $L \leq 2$  restriction, in contrast to  $L \leq 3$  for other nuclei.

In the considered cases the binding energies of the Pauli-forbidden  $1s_{1/2}$  states range from 22 MeV ( $n$ - $^{17}\text{B}$ ) to 37 MeV ( $n$ - $^{16}\text{O}$ ), and from 4 MeV ( $n$ - $^9\text{Li}$ ) to 32 MeV ( $n$ - $^{16}\text{O}$ ) in  $1p_j$  states.

The calculated ground-state binding energies are collected in Table I. The numerical accuracy is 1 ( $^{19}\text{B}$ ) to 10 keV ( $^{18}\text{O}$ ). The predictions are in good agreement with previous calculations where available [24, 29, 30], the remaining discrepancies most likely being due to differences in the included partial waves, two-neutron potential, and even parameter value roundoff. The experimental values from Ref. [31] are listed as well. The aim is not to fit these values, but they turn out to be quite close to one of the models used to remove Pauli-forbidden states. However, the most important message from Table I is that the SS

TABLE I. Ground-state binding energies  $|E_B|$  (in MeV) for the considered nuclei calculated using PP and SS models. The last line  $^{18}\text{O}$  results are obtained including also  $L = 3$  waves with the same parameters as in  $L = 2$  waves. The experimental data are from Ref. [31]. The experimental value for  $^{19}\text{B}$  is a compilation from several measurements and theoretical evaluations, having a large uncertainty of about 0.4 MeV; see also Ref. [29].

	PP	SS	Exp.
$^{19}\text{B}$	0.185	0.383	0.145
$^{11}\text{Li}$	0.296	0.855	0.369
$^{20}\text{C}$	2.675	3.644	3.560
$^{16}\text{C}$	4.342	5.299	5.468
$^{18}\text{O}$	11.458	12.773	12.188
$^{18}\text{O}$	11.550	12.917	12.188

model systematically predicts larger binding energies as compared to PP.

Noteworthy, all of these core-neutron systems support a virtual or weakly bound  $2s_{1/2}$  state. Together with the virtual two-neutron  $^1S_0$  state this fulfills the condition for the manifestation of the Efimov physics [27]. As a consequence, the three-body ground states emerge already under restriction to  $L = 0$  partial waves. The universality predicts low sensitivity to the short-range details, and indeed the binding energies calculated with solely  $L = 0$  partial waves in PP and SS models are very similar. It is interesting to study how the differences between the PP and SS approaches emerge starting from this roughly universal situation. The results for three-body binding energy calculations including the neutron-core interaction in partial waves with  $L \leq L_{\text{max}}$  are shown in Fig. 4. The two-neutron potential is taken up to  $L = 3$ , but  $L > 0$  waves yield only small contribution not affecting the picture qualitatively. Except for  $^{11}\text{Li}$ , all  $1p_j$  waves contain Pauli-forbidden states, the interaction is predominantly Pauli-repulsive with little effect for the binding energy. In contrast,  $L = 2$  core-neutron waves contain no Pauli-forbidden states and yield quite appreciable contribution. Most importantly, in the SS model it is considerably larger than in PP, and this is decisive for the SS-PP difference. The changes due to  $L = 3$  waves are small. In the  $^{11}\text{Li}$  case, shown in the inset of Fig. 4, the  $1p_{1/2}$  state has no Pauli repulsion and therefore already  $L_{\text{max}} = 1$  results show an increase of the binding energy, further enhanced by  $L = 2$  waves. Again, in the SS model the rise of the binding energy is considerably larger than in PP.

Thus, Fig. 4 indicates that three-body ground state energies calculated using SS and PP models are close as long as only low partial waves containing Pauli-forbidden states are included. However, the interplay of lower and higher partial waves leads to the binding energy increase that is significantly larger for SS. The reason might be different wave functions, i.e., different weights

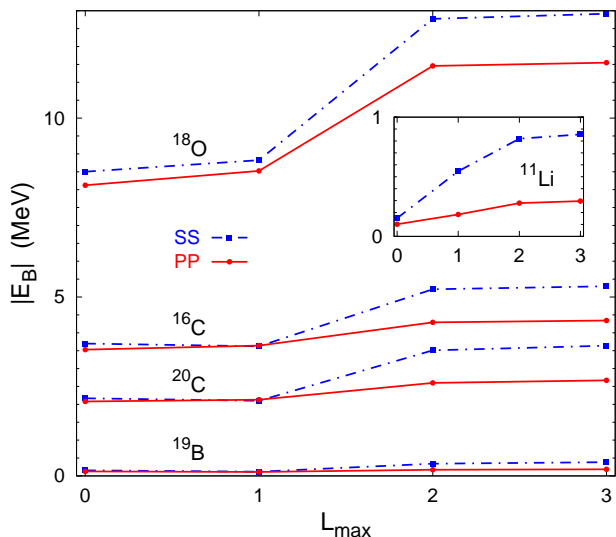


FIG. 4. (Color online) Ground-state binding energy of  $^{19}\text{B}$ ,  $^{11}\text{Li}$ ,  $^{20}\text{C}$ ,  $^{16}\text{C}$ , and  $^{18}\text{O}$  nuclei, calculated including different number of angular momentum states. The predictions of SS and PP models are compared. The lines are for guiding the eye only.

of various momentum components. A global measure for the low/high momentum components is the expectation value of the kinetic energy  $E_K = \langle \Psi | H_0 | \Psi \rangle$ . It is presented in Fig. 5 for  $^{11}\text{Li}$  and  $^{16}\text{C}$ ; the remaining cases are qualitatively similar to  $^{16}\text{C}$ . It reveals drastic differences already in low partial waves, the kinetic energy in the PP model being considerably higher than in SS. When higher partial waves without Pauli repulsion are included,  $E_K$  rises more strongly in the SS model. For  $^{11}\text{Li}$  this happens at  $L_{\text{max}} = 1$  while for the remaining cases at  $L_{\text{max}} = 2$ . The difference in  $E_K$  by far exceeds the one in binding energy, indicating that the expectation value of the potential energy  $E_V = E_B - E_K$  in the PP model is also higher in absolute value despite that the binding energy is lower, only  $^{11}\text{Li}$  being the exception. Thus, the observed difference in binding energies is a result of partial cancellations between kinetic and potential energies. A conjecture is that the PP model, explicitly imposing orthogonality to the Pauli-forbidden state, induces higher momentum components, leading to larger  $E_K$ . On the other hand, the repulsive core of the SS model leads to lower  $|E_V|$  and possibly increases the weight of larger distance components in low partial waves, thereby making the coupling to higher waves more efficient, and increasing their effect both for  $E_K$  and  $E_B$  as observed in Figs. 4 and 5. For example, in  $^{16}\text{C}$  the weight of the dominating  $L = 0$  and  $L = 2$  core-neutron components is around 62% and 35% in PP but 51% and 46% in SS model, respectively. The remaining 3% are distributed among  $L = 1$  and  $L = 3$  waves.

The core-neutron relative momentum distributions are compared in Fig. 6 for the example of  $^{16}\text{C}$ , and turn out

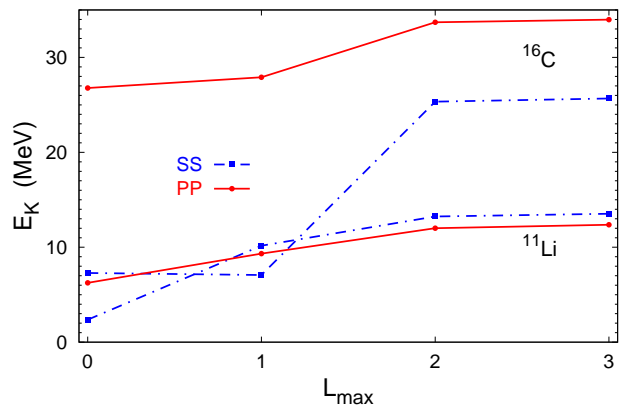


FIG. 5. (Color online) Kinetic energy expectation value for ground state of  $^{11}\text{Li}$  and  $^{16}\text{C}$  nuclei, calculated including different number of angular momentum states. The predictions of SS and PP models are compared. The lines are for guiding the eye only.

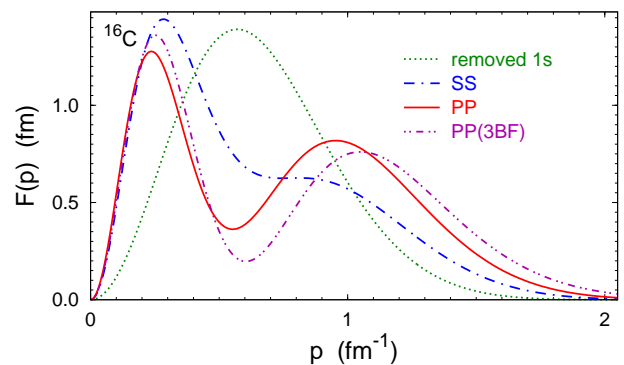


FIG. 6. (Color online) Core-neutron relative momentum distribution in the ground state of  $^{16}\text{C}$  and in the Pauli-forbidden  $1s_{1/2}$  state of  $^{15}\text{C}$  (dotted curve). Results of SS (dashed-dotted curve), PP (solid curve), and PP+3BF (double-dotted-dashed curve) models are compared.

to be quite different. The normalization is  $\int_0^\infty F(p) dp = 1$ . In order to eliminate the possible effect due to the binding energy mismatch, a phenomenological three-body force (3BF) is added to the PP Hamiltonian; its form and resulting equations can be found in Ref. [32]. With parameters  $\Lambda = 2 \text{ fm}^{-1}$  and  $w_3 = -6.2 \text{ MeVfm}^6$  in the convention of Ref. [32] the PP+3BF model binding energy coincides with the one of SS. The resulting momentum distribution is shifted towards larger momenta but nevertheless remains closer to the one by PP. For curiosity, the momentum distribution of the Pauli forbidden  $1s_{1/2}$  state is shown as well. Its maximum almost coincides with local minimum in PP and PP+3BF models, consistently with a vanishing overlap  $\langle \phi_P^{Lj} | \Psi \rangle$ . This does not take place in the SS model where the weight of this overlap is 0.166, the momentum distribution does not show a deep minimum and has considerably lower

TABLE II. Binding energies  $|E_B|$  (in MeV) for excited states of the considered nuclei calculated using PP and SS models. The experimental data are from Ref. [31]. The  $^{18}\text{O}(0_2^+)$  in the theoretical model corresponds to the experimental  $^{18}\text{O}(0_3^+)$  state as explained in Ref. [30].

	PP	SS	Exp.
$^{20}\text{C}(2^+)$	1.433	2.323	1.942
$^{16}\text{C}(2^+)$	3.337	4.058	3.702
$^{18}\text{O}(2^+)$	10.281	11.078	10.206
$^{20}\text{C}(0_2^+)$	0.668	0.632	
$^{16}\text{C}(0_2^+)$	2.490	1.918	2.441
$^{18}\text{O}(0_2^+)$	7.823	7.133	6.852
$^{16}\text{C}(2_2^+)$	1.614	1.621	1.482
$^{18}\text{O}(2_2^+)$	8.456	8.601	8.268
$^{16}\text{C}(3^+)$	1.617	1.706	1.380
$^{18}\text{O}(3^+)$	7.429	7.605	6.811
$^{16}\text{C}(4^+)$	1.668	1.716	1.326
$^{18}\text{O}(4^+)$	8.624	8.810	8.633

high-momentum tail.

Except for very weakly bound  $^{11}\text{Li}$  and  $^{19}\text{B}$  systems, the other considered nuclei support excited states, at least those with total spin and parity  $J^\Pi = 2^+$  and  $0^+$ ; the later will be labeled  $0_2^+$  in order to distinguish from the ground state. For  $^{16}\text{C}$  and  $^{18}\text{O}$  few more excited states are available. The predictions for their binding energies are collected in Table II. Interaction in partial waves with  $L = 2$  is necessary for these states to appear. Their binding energies again show a systematic behavior, in the SS model being larger for  $2^+$  states by roughly 0.8 MeV but smaller by up to 0.7 MeV for  $0_2^+$  states as compared to PP. Noteworthy, both models predict a very weakly bound  $^{20}\text{C}(0_2^+)$  state, 50 to 90 keV below the  $n\text{-}^{19}\text{C}$  threshold; this state is not known experimentally. For definite conclusions a more refined  $n\text{-}^{18}\text{C}$  potential, especially in  $L > 0$  waves, possibly including also the core excitation, is needed, which is beyond the goals of the present study. For further  $^{16}\text{C}$  and  $^{18}\text{O}$  states the SS binding energies are slightly larger, but the difference is not significant. This reduced sensitivity probably can be explained by the fact that for higher  $J$  values the partial waves containing Pauli-forbidden states must couple with larger spectator orbital momentum  $l$ , and their weight in the bound-state wave function is small. For example, in the  $^{18}\text{O}(4^+)$  state the weight of  $L \leq 1$  waves is well below 0.5%. Regarding the experimental data, there is no clear preference of any of the models. The predicted binding energies are roughly consistent with the data for  $^{18}\text{O}$ , while for higher  $^{16}\text{C}$  states they are slightly overestimated, the experimental data being closer to the  $^{15}\text{C}$  threshold located at 1.218 MeV.

Regarding the scattering calculations, the above neutron-nucleus potentials are only suitable at very-low energies since being real they do not account for inelastic

TABLE III. Scattering length (in units of fm) for neutron scattering off different two-cluster nuclei (in the ground state) in a given total angular momentum and parity state. The numerical accuracy is better than 1%.

	$J^\Pi$	PP	SS
$n\text{-}^{19}\text{C}$	$0^+$	16.4	26.6
$n\text{-}^{19}\text{C}$	$1^+$	9.25	9.25
$n\text{-}^{15}\text{C}$	$0^+$	4.84	7.74
$n\text{-}^{15}\text{C}$	$1^+$	7.40	7.39
$n\text{-}^{17}\text{O}$	$2^+$	4.23	3.73
$n\text{-}^{17}\text{O}$	$3^+$	5.30	5.26

TABLE IV.  $^{16}\text{Be}$  resonance energies and widths (both in MeV) calculated using PP and SS models. The experimental data are from Ref. [33].

	PP		SS		Exp.	
	$E_R$	$\Gamma$	$E_R$	$\Gamma$	$E_R$	$\Gamma$
$^{16}\text{Be}(0^+)$	2.08	0.27	1.69	0.25	0.84	0.32
$^{16}\text{Be}(2^+)$	2.91	0.49	2.69	0.59	2.15	0.95

processes. Here they are applied for the neutron scattering off a core plus neutron system at zero energy. The predicted values for scattering lengths  $a_{12}(J^\Pi)$  are collected in Table III. In channels with higher  $J$  values the spins of the neutrons are aligned, producing the Pauli repulsion at the level of external neutrons with very little sensitivity to the details of the interaction. In fact, in those channels  $a_{12}(J^\Pi)$  is very close to the neutron-core scattering length as observed also in Ref. [28]. In channels with lower  $J$  values  $a_{12}(J^\Pi)$  is affected by the state closest to the threshold, where the differences in binding energy predictions of PP and SS models are reflected in the  $a_{12}(J^\Pi)$  differences, with the lower binding energy corresponding to the larger scattering length. In particular, a very shallow  $^{20}\text{C}(0_2^+)$  state leads to large values of  $a_{12}(0^+)$  in  $n\text{-}^{19}\text{C}$  scattering.

### C. $^{16}\text{Be}$ resonances

The  $n\text{-}^{14}\text{Be}$  potential parameters are taken from Refs. [11, 12], reproducing spectrum of  $^{15}\text{Be}$   $d$ -wave resonances. Partial waves with  $L \leq 3$  are included. The  $^{16}\text{Be}$  resonance parameters are extracted using Eq. (5), about five terms are needed to achieve the convergence of results. The numerical accuracy is better than 0.02 MeV. The resonance positions and widths are collected in Table IV.

For both  $^{16}\text{Be}$  states  $0^+$  and  $2^+$  the SS model predicts the resonance at lower energy than PP. This is fully consistent with the same  $J^\Pi$  bound-state results, where the SS model predicted more binding. As in Refs. [11, 12], the chosen two-body potentials predict the resonances at

higher energies than experimental data, a possible remedy being an attractive three-body force. On the other hand, except for a rather well established  $^{15}\text{Be}(\frac{5}{2}^+)$  resonance, the two-body interaction is not well constrained by the data.

#### IV. DISCUSSION AND CONCLUSIONS

Faddeev-type equations for bound and scattering states in three-body systems consisting of a nucleus and two nucleons were solved in the momentum-space partial wave representation. Two methods for eliminating the Pauli-forbidden states were compared, either projecting those states out by a nonlocal projection term in the two-body potential, or by a supersymmetric transformation of the two-body potential. While some previous studies of this type exist for weakly bound halo nuclei, this work presents a more systematic study involving elastic and inelastic deuteron scattering, excited and resonant states.

Results for the deuteron- $^4\text{He}$  elastic scattering and breakup clearly indicate that the PP method is favored by the experimental data while SS and RC methods are close to each other and fail similarly. For bound-states and resonances there is no clear preference of the method,

but systematic differences between them are established: the SS method predicts larger binding energy (lower resonance position) for the ground state and  $2^+$  excited state, while the PP method leads to larger binding energy for  $0_2^+$  excited states. These differences in binding energy predictions are reflected in the respective scattering lengths for the neutron scattering off the core plus neutron system. The differences are small as long as only low partial waves containing Pauli-forbidden states are included, but the interplay of lower and higher partial waves leads to the binding energy increase that is significantly larger for SS. Furthermore, the expectation value for the kinetic energy is typically higher in the PP method, with sizable differences in momentum distributions as well. This could show up in breakup reactions, where the amplitudes depend on the momentum distributions in the bound state [32]. The higher excited states have quite small components with low partial waves and therefore show only mild difference between PP and SS treatments. Noteworthy, in both methods a very weakly bound  $^{20}\text{C}(0_2^+)$  excited state emerges that is not yet known experimentally. A more definite conclusions regarding this (and some other) exotic nuclei require better constrained nucleon-nucleus potentials.

- 
- [1] N. K. Timofeyuk and R. C. Johnson, *Progress in Particle and Nuclear Physics* **111**, 103738 (2020).
- [2] V. Kukulín, V. Krasnopolsky, V. abnd Voronchev, and P. Sazonov, *Nuclear Physics A* **417**, 128 (1984).
- [3] N. W. Schellingerhout, L. P. Kok, S. A. Coon, and R. M. Adam, *Phys. Rev. C* **48**, 2714 (1993).
- [4] I. J. Thompson, B. V. Danilin, V. D. Efros, J. S. Vaagen, J. M. Bang, and M. V. Zhukov, *Phys. Rev. C* **61**, 024318 (2000).
- [5] E. Garrido, D. Fedorov, and A. Jensen, *Nuclear Physics A* **617**, 153 (1997).
- [6] E. Garrido, D. Fedorov, and A. Jensen, *Nuclear Physics A* **650**, 247 (1999).
- [7] D. Baye, *Phys. Rev. Lett.* **58**, 2738 (1987).
- [8] M. Hesse, D. Baye, and J.-M. Sparenberg, *Physics Letters B* **455**, 1 (1999).
- [9] A. Deltuva, *Phys. Rev. C* **74**, 064001 (2006).
- [10] E. O. Alt, P. Grassberger, and W. Sandhas, *Nucl. Phys.* **B2**, 167 (1967).
- [11] A. E. Lovell, F. M. Nunes, and I. J. Thompson, *Phys. Rev. C* **95**, 034605 (2017).
- [12] J. Casal and J. Gómez-Camacho, *Phys. Rev. C* **99**, 014604 (2019).
- [13] L. D. Faddeev, *Zh. Eksp. Teor. Fiz.* **39**, 1459 (1960) [*Sov. Phys. JETP* **12**, 1014 (1961)].
- [14] A. Deltuva, *Phys. Rev. C* **97**, 034001 (2018).
- [15] J. R. Taylor, *Nuovo Cimento B* **23**, 313 (1974); M. D. Semon and J. R. Taylor, *Nuovo Cimento A* **26**, 48 (1975).
- [16] E. O. Alt and W. Sandhas, *Phys. Rev. C* **21**, 1733 (1980).
- [17] A. Deltuva, A. C. Fonseca, and P. U. Sauer, *Phys. Rev. C* **71**, 054005 (2005).
- [18] R. Machleidt, *Phys. Rev. C* **63**, 024001 (2001).
- [19] A. Deltuva, *Phys. Rev. C* **79**, 054603 (2009).
- [20] W. Gruebler, R. E. Brown, F. D. Correll, R. A. Hard-ekopf, N. Jarmie, and G. G. Ohlsen, *Nucl. Phys.* **A331**, 61 (1979).
- [21] I. Koersner, L. Glantz, A. Johansson, B. Sundqvist, H. Nakamura, and H. Noya, *Nucl. Phys.* **A286**, 431 (1977).
- [22] P. Niessen, S. Lemaitre, K. R. Nyga, G. Rauprich, R. Reckenfelderbäumer, L. Sydow, H. Paetz gen. Schieck, and P. Doleschall, *Phys. Rev. C* **45**, 2570 (1992).
- [23] H. Kamada, S. Oryu, and A. Nogga, *Phys. Rev. C* **62**, 034004 (2000).
- [24] I. J. Thompson and M. V. Zhukov, *Phys. Rev. C* **49**, 1904 (1994).
- [25] F. Nunes, J. Christley, I. Thompson, R. Johnson, and V. Efros, *Nucl. Phys. A* **609**, 43 (1996).
- [26] I. Thompson, F. Nunes, and B. Danilin, *Computer Physics Communications* **161**, 87 (2004).
- [27] A. Jensen, K. Risager, D. Fedorov, and E. Garrido, *Reviews of Modern Physics* **76**, 215 (2004).
- [28] A. Deltuva, *Phys. Lett. B* **772**, 657 (2017).
- [29] E. Hiyama, R. Lazauskas, J. Carbonell, and T. Frederico, *Phys. Rev. C* **106**, 064001 (2022).
- [30] N. Li, X.-R. Zhao, R. Zhang, L.-K. Wu, M.-J. Lyu, J.-J. He, W.-Y. Tong, Z.-Y. Zhang, and Y.-X. Li, *Phys. Rev. C* **112**, 024004 (2025).
- [31] <https://www.nndc.bnl.gov/ensdf/>.
- [32] A. Deltuva, *Phys. Rev. C* **87**, 034609 (2013).
- [33] B. Monteagudo, F. M. Marqués, J. Gibelin, N. A. Orr, A. Corsi, Y. Kubota, J. Casal, J. Gómez-Camacho, G. Authelet, H. Baba, C. Caesar, D. Calvet, A. Delbart,

M. Dozono, J. Feng, F. Flavigny, J.-M. Gheller, A. Giganon, A. Gillibert, K. Hasegawa, T. Isobe, Y. Kanaya, S. Kawakami, D. Kim, Y. Kiyokawa, M. Kobayashi, N. Kobayashi, T. Kobayashi, Y. Kondo, Z. Korkulu, S. Koyama, V. Lapoux, Y. Maeda, T. Motobayashi, T. Miyazaki, T. Nakamura, N. Nakatsuka, Y. Nishio, A. Obertelli, A. Ohkura, S. Ota, H. Otsu, T. Ozaki, V.

Panin, S. Paschalis, E. C. Pollacco, S. Reichert, J.-Y. Rousse, A. T. Saito, S. Sakaguchi, M. Sako, C. Santamaria, M. Sasano, H. Sato, M. Shikata, Y. Shimizu, Y. Shindo, L. Stuhl, T. Sumikama, Y. L. Sun, M. Tabata, Y. Togano, J. Tsubota, T. Uesaka, Z. H. Yang, J. Yasuda, K. Yoneda, and J. Zenihiro, *Phys. Rev. Lett.* **132**, 082501 (2024).